Inter-cage dynamics in structure I, II, and H fluoromethane hydrates as studied by NMR and molecular dynamics simulations

ARTICLE *in* THE JOURNAL OF CHEMICAL PHYSICS · JUNE 2014

Impact Factor: 2.95 · DOI: 10.1063/1.4874636

7 AUTHORS, INCLUDING:

Alondra Torres Trueba
Delft University of Technology
5 PUBLICATIONS **50** CITATIONS

SEE PROFILE

Cor Peters
Petroleum Institute (UAE)
332 PUBLICATIONS **6,356** CITATIONS

SEE PROFILE

John A. Ripmeester
National Research Council Canada
713 PUBLICATIONS **15,407** CITATIONS

SEE PROFILE

Inter-cage dynamics in structure I, II, and H fluoromethane hydrates as studied by NMR and molecular dynamics simulations

Alondra Torres Trueba, Maaike C. Kroon, Cor J. Peters, Igor L. Moudrakovski, Christopher I. Ratcliffe, Saman Alavi, and John A. Ripmeester

Citation: The Journal of Chemical Physics **140**, 214703 (2014); doi: 10.1063/1.4874636
View online: http://dx.doi.org/10.1063/1.4874636
View Table of Contents: http://scitation.aip.org/content/aip/journal/jcp/140/21?ver=pdfcov
Published by the AIP Publishing

Inter-cage dynamics in structure I, II, and H fluoromethane hydrates as studied by NMR and molecular dynamics simulations

Alondra Torres Trueba,[1,2] Maaike C. Kroon,[2] Cor J. Peters,[2,3] Igor L. Moudrakovski,[1,a)] Christopher I. Ratcliffe,[1] Saman Alavi,[1,4] and John A. Ripmeester[1,b)]
[1]*Steacie Institute for Molecular Sciences, National Research Council Canada, Ottawa, Ontario, K1A 0R6, Canada*
[2]*Eindhoven University of Technology, Department of Chemical Engineering and Chemistry, Separation Technology Group, Den Dolech 2, 5612 AZ Eindhoven, The Netherlands*
[3]*The Petroleum Institute, Chemical Engineering Department, P. O. Box 2533, Abu Dhabi, United Arab Emirates*
[4]*Department of Chemistry, University of Ottawa, Ottawa, Ontario K1N 6N5, Canada*

(Received 3 February 2014; accepted 15 April 2014; published online 3 June 2014)

Prospective industrial applications of clathrate hydrates as materials for gas separation require further knowledge of cavity distortion, cavity selectivity, and defects induction by guest-host interactions. The results presented in this contribution show that under certain temperature conditions the guest combination of CH_3F and a large polar molecule induces defects on the clathrate hydrate framework that allow intercage guest dynamics. ^{13}C NMR chemical shifts of a CH_3F/CH_4/TBME sH hydrate and a temperature analysis of the ^2H NMR powder lineshapes of a CD_3F/THF sII and CD_3F/TBME sH hydrate, displayed evidence that the populations of CH_4 and CH_3F in the D and D′ cages were in a state of rapid exchange. A hydrogen bonding analysis using molecular dynamics simulations on the TBME/CH_3F and TBME/CH_4 sH hydrates showed that the presence of CH_3F enhances the hydrogen bonding probability of the TBME molecule with the water molecules of the cavity. Similar results were obtained for THF/CH_3F and THF/CH_4 sII hydrates. The enhanced hydrogen bond formation leads to the formation of defects in the water hydrogen bonding lattice and this can enhance the migration of CH_3F molecules between adjacent small cages. © *2014 AIP Publishing LLC*. [http://dx.doi.org/10.1063/1.4874636]

I. INTRODUCTION

Clathrate hydrates are crystalline inclusion compounds where guest molecules are trapped in cages formed from hydrogen bonded water molecules.[1–3] There are three main families of clathrate hydrates, the cubic structures I (sI) and II (sII) which require two kinds of water cages to give a space-filling lattice, and the hexagonal structure H (sH), which requires three cages (5^{12} D, $4^3 5^6 6^3$ D′, $5^{12}6^8$ E).[4] Clathrate hydrates of each type occur naturally with different hydrocarbon guests; sI with methane (CH_4) as main guest, the other two structures with the small cages filled mostly with CH_4 and the larger cages with propane, isobutane, methyl butanes, and methyl substituted cycloalkanes.[5,6] Prospective industrial application of clathrate hydrates as materials for gas separation[7–10] and as storage and transport medium of energy carrying gases have been considered.[11] However, high pressure and low temperature conditions are required for hydrate formation,[1] clathrate hydrates contain relatively low mass percent gas content,[12] and the kinetics of hydrate formation is nonuniform[13] increasing the difficulties to achieve complete hydrate formation in one step. Therefore, there is the need to apply a crystal engineering approach in order to modify the crystal structure and properties of clathrate hydrates with the aim to make them more suitable for industrial applications.

Previous work has shown that fluoromethane (CH_3F) is a viable small cage (D, 5^{12}) guest in sI,[14,15] sII,[16,17] and sH.[18] Nevertheless, no attempts have been made to understand the influence of CH_3F on the behavior of gas uptake and hydrate stability. Consequently, in the current work the effect of CH_3F on the properties of sII and sH clathrate hydrates are studied. The technique of choice was solid state ^{13}C NMR spectroscopy, as it has been shown that in favorable cases CH_4 guests in the sH D and D′ cages can be distinguished from the ^{13}C resonance lines.[19] In this contribution, we show that at temperatures above a certain threshold, the combination of CH_3F and a large polar guest induce defects in the hydrate framework that allow intercage guest dynamics. Molecular dynamics simulations and ^2H NMR are used to support the conclusions.

^{13}C NMR spectra of CH_3F in clathrate hydrates have not been previously studied however they were expected to be more complex than CH_4 spectra because of the strong coupling of ^{13}C with ^{19}F.[20] Spinning under magic angle spinning (MAS) conditions can lead to complex spectra due to the interference effects among the various spin tensors (dipolar, *J*-coupling, and anisotropic chemical shift) as modified by

a)Present address: Max Planck Institute for Solid State Research, Stuttgart 70569, Germany.
b)Author to whom correspondence should be addressed. Electronic mail: John.Ripmeester@nrc-cnrc.gc.ca. Tel.:+1 6139932011; Fax.:+1 6139987833.

molecular motion.[21] The cage geometry determines whether the dynamics of the guest is isotropic or not, and to a lesser extent, the correlation time for the motion.

The CH_4 and CH_3F molecules differ in size and dipole moment. We use molecular dynamics simulation to compare the rotational dynamics of CH_4 and CH_3F in the D and D′ cages of sH and in the D cage of sII hydrate at different temperatures and pressures. We also study their effect on the hydrogen bonding between the guest in the large cage and the water molecules of the large cage.[4] In addition, the free energy of substitution of CH_4 with CH_3F in the D and D′ cages of sH clathrate hydrate was calculated via molecular dynamic (MD) thermodynamic integration calculations to determine whether there is cage selectivity between these two guests. Thermodynamic integration has been previously used to study the stability and occupancy of H_2 in sII clathrate hydrates,[22] the stability of rare gases in sH,[23] CH_4 occupancy and stability in sH clathrate hydrate,[24] and most recently the carbon dioxide (CO_2) substitution in sI clathrate hydrates.[10,25]

II. MATERIALS AND METHODS

A. Materials

Methane (CH_4) was obtained from Praxair (UHP grade), fluoromethane-d_3 (CD_3F) (99%), and fluoromethane (CH_3F) (99%) were obtained from Synquest Labs. Tretrahydrofuran (THF) (99%), methylcyclohexane (MCH) (99%), and tert-butylmethylether (TBME) (99%) were purchased from Sigma Aldrich. All the samples were prepared with distilled water and all the chemicals were used without any further purification.

B. Sample preparation

The sI clathrate hydrates of CH_3F, double sII clathrate hydrates of CH_3F and tetrahydrofuran (THF) and double sH clathrate hydrates of CH_3F and tetra-butylmethylether (TBME), and CH_3F and methylcyclohexane (MCH) were prepared in a Pyrex tube attached to a vacuum system by means of a flexible stainless steel tube. The sI clathrate hydrate was formed by placing in contact finely powdered ice and CH_3F gas at a pressure of ∼500 torr. The sII and sH clathrate hydrates were formed by placing finely powdered ice and sufficient quantities of liquid THF, TBME, or MCH in contact with CH_3F gas (−500 torr) to give a water/large molecule mole ratio of 1:20. Afterwards, the sample tubes were sealed and then alternately cooled and shaken on a Vortex mixer. The samples were conditioned at −3 °C for seven days. Some helium gas at low pressure was admitted to provide good thermal contact between the sample and the tube walls. Similar procedures were followed to prepare the CD_3F sI clathrate hydrates, double CD_3F-THF sII clathrate hydrates, and double CD_3F-TBME sH clathrate hydrates.

Mixed sH clathrate hydrates of CH_3F, CH_4, and TBME were synthesized from a mixture of solid particles of frozen TBME and water mixture. The solid particles were formed by gravimetrically preparing a liquid solution of TBME and water, the amount of TBME was ∼55% in excess of the stoichiometric concentration for sH. The solution was then frozen and crushed under liquid nitrogen (LN). The crushed particles were poured into a chilled 50 cm^3 pressure vessel; approximately 4.7 g of solid particles were used. In order to prevent the melting of the solid material the loading was performed in a freezer at 253 K. After the loading, the vessel was sealed and immersed in a constant temperature bath containing a water-methanol mixture and connected to a valve and pressure transducer. The cell was slowly purged with the gas mixture three times, and then pressurized slowly to 50 bar. The sample was kept at 253 K and 50 bar for about 5–6 days. The gas mixture ∼50/50 mol% of CH_4/CH_3F was prepared gravimetrically. At the end of the formation period the gas was released and the hydrate sample was collected at LN temperature (77 K) and kept in LN for subsequent analysis.

C. NMR methods

The ^{13}C NMR spectra were recorded for pure CH_3F sI hydrates, double sII hydrates of CH_3F and THF, sH hydrates of CH_3F and TBME, sH hydrates of CH_3F and MCH, and for the mixed sH hydrates of CH_3F, CH_4, and TBME. The spectra were collected on a Bruker Avance III 400 MHz instrument at ^{13}C Larmor frequency of 100.6 MHz (magnetic field of 9.4 T). The spinning speed and the temperature inside the probe were controlled using standard Bruker equipment. Prior to the NMR experiments the hydrate samples were ground under LN and packed in 7-mm zirconia rotors. The measurements were performed at temperatures from 183 K to 253 K and 3-kHz spinning speed. Both Bloch decay (single-pulse excitation) and cross polarization (CP) experiments were performed in order to differentiate the signals from the solid and liquid phases. Bloch decay experiments used a 90° pulse of 5 μs and composite pulse proton high power decoupling (HPDEC). The high frequency ^{13}C NMR resonance peak of adamantane (38.56 ppm from tetramethylsilane (TMS), $\delta = 0.0$ ppm) at 298 K and was used as the secondary external chemical shift reference.

Static solid state ^2H NMR spectra for sI hydrates of CD_3F, double sII hydrates of CD_3F-THF, and double sH hydrates of CD_3F-TBME were obtained at 46.05 MHz on a Bruker AMX-300 (magnetic field of 7.04 T) and at 61.42 MHz on a Bruker Avance-III-400 (magnetic field of 9.4 T) instruments, using a quadrupole echo pulse sequence[26] with echo delay time of 35 μs, and $\pi/2$-pulses of 3.3 μs and 2.7 μs, respectively. The various temperatures were obtained using a modified Bruker probe and a Eurotherm BVT3000 controller using cold flowing nitrogen gas. Measurements at 77 K were obtained with the sample immersed in liquid nitrogen. Between 8 and 128 accumulations were obtained with relaxation delays ranging from 5 to 60 s.

D. Molecular dynamics methods

Simulations of the sH hydrates were performed in a 3 × 3 × 3 replica of the unit cell with initial dimensions set at 36.84 × 31.09 × 29.64 Å^3 and sII hydrates in a 2 × 2 × 2 replica of the unit cell with initial dimensions of 34.68 × 34.68

$\times$ 34.68 Å^3, imposing periodic boundary conditions in all cases. The DL_POLY molecular dynamics simulation package version 2.20[27] was used in the *NpT* ensemble using the Nosé–Hoover thermostat-barostat algorithm[28] with thermostat and barostat relaxation times of 0.2 and 0.5 ps, respectively. Time steps of 1 fs are used in all simulations. The initial positions of the water oxygen atoms of the hydrate lattice were obtained from the crystallographic structures of sH[29] and sII hydrate.[30] The disordered water hydrogen atoms were arranged about water oxygen sites subjected to the constrains of the Bernal-Fowler ice rules[31] via a unit-cell dipole-moment minimizing Monte Carlo calculation.

The TIP4P potential was used for water.[32] The structures of TBME, THF, and CH_3F were determined by energy optimization using density function theory at the B3LYP/6-311++G(*d*,*p*) level with the Gaussian 03 suite of programs.[33] The electrostatic point charges on the optimized TBME, THF, and CH_3F molecules are estimated from "charges from electrostatic potential grid" (CHELPG) method as implemented in Gaussian 03. The intermolecular van der Waals interaction parameters are taken from the general AMBER force field (GAFF).[34] Methane molecules modeled with the Murad-Gubbins single-point potential[35] (in the free energy calculations) and the TRAPPE all-atom potential[35] (in hydrogen bonding and guest dynamics studies). Standard combination rules, $\varepsilon_{ij} = (\varepsilon_{ii}\varepsilon_{jj})^{1/2}$ and $\sigma_{ij} = (\sigma_{ii}+\sigma_{jj})/2$ were used to derive the Lennard-Jones potential parameters between unlike atom-type force centers *i* and *j*. The Ewald summation method was used to calculate long-range Coulombic interactions and all intermolecular interactions in the simulation box within a cutoff distance of 13.0 Å. Table S1 of the supplementary material[36] shows the atomic electrostatic point charges and the Lennard-Jones parameters of the molecules used in the simulations. The internal degrees of motion of molecules in the clathrate hydrates were considered to be frozen and the molecules moved as a rigid unit in the simulations.

In the sH simulations, initially, all large cages are occupied by a single TBME molecule (27 molecules in total), whereas all small and medium cages are occupied by either CH_3F or CH_4 molecules (135 molecules in total, of which 81 are in the small cages and 54 are in the medium cages). In the sII simulations, all large cages are occupied by a single THF molecule (64 molecules in total), whereas all small cages are occupied by either CH_3F or CH_4 molecules (132 molecules in total). These configurations with all small cages occupied by guests are hypothetical since experimentally some fraction of the small/medium cages remains vacant.

Two sets of simulation studies were performed. In the first set, we studied hydrogen bonding of the ether oxygen (OS) of TBME and THF with water in the binary systems of sH and sII with CH_3F or CH_4. We previously found that the shape and interaction of the small molecule "help-gas" guests can significantly affect the hydrogen bonding of the large cage guests.[4] This large-guest hydrogen bonding with framework water molecules can in turn lead to the formation of defects in the water hydrogen bonding network which affects the stability of the hydrate phase and the dynamical behavior of the water molecules and small cage guests. We shall use the results of these simulations in the interpretation of some of the experimental NMR results.

Constant pressure-temperature *NpT* simulations were performed for the sH and sII hydrates with CH_3F and all-atom representation of the CH_4 molecules. Hydrogen bond dynamics and small guest rotation dynamics were extracted from constant energy/volume *NVE* simulations and were executed starting with the final *NpT* configurations previously described. The *NVE* simulations were performed for a total time of 600 ps, with the first 100 ps used for equilibration. Pressures from 1 to 50 bar at two temperatures 183 and 253 K were studied for each hydrate system in sH, and for the systems in sII simulations were carried out at 250 and 281 K and 1 bar. The guests were considered hydrogen bonded to a water molecule if the OS atom distance to a hydrogen atom of water (HW) was less than 2.1 Å. The average probability of hydrogen bond formation was calculated by averaging the ratio of times during the simulation that TBME or THF were hydrogen bonded to the cage water molecules.

In a second series of molecular dynamics simulations, we determined the free energy for substitution of CH_4 guests in the small and medium cages of the binary sH hydrate with TMBE with CH_3F guests using the thermodynamic integration method. Simulations were carried out for 500 ps with the first 200 ps used for equilibration.

The MD simulations are used to determine the Gibbs free energy associated with the following reaction:

$$\text{sH clathrate}[\text{TBME}(L) + 5\text{CH}_4(S/M)] + 5\text{CH}_3\text{F(g)} \rightarrow \text{sH clathrate}[\text{TBME}(L) + 5\text{CH}_3\text{F}(S/M)] + 5\text{CH}_4\text{(g)}, \quad (1)$$

where 5 CH_3F gas molecules at a temperature *T* and pressure *p* replace 5 CH_4 molecules from the small and medium cages of the sH clathrate hydrate. The CH_4 molecules originally in the hydrate phase are subsequently released to the gas phase. The methodology for the thermodynamics integration method for the free energy calculations is standard and described in the supplementary material.[36]

III. RESULTS AND DISCUSSION

A. NMR studies

Zilm *et al.*[20] reported the low temperature ^{13}C spectrum of CH_3F in an argon matrix. The spectrum is a doublet due to ^{13}C–^{19}F dipolar coupling (D) plus anisotropic *J* coupling (ΔJ). Spin coupling parameters for ^{19}F in a rigid C–F bond are: $D_{C-F} = 10$ kHz, $J_{C-F} \sim 158$ Hz, $\Delta\upsilon_{13C} = 1800$ Hz (at 20.12 MHz = 1.88 T) therefore $\Delta\delta = \sim 90$ ppm, $\Delta J = 1200 \pm 1200$ Hz. With MAS of the rigid ^{13}C–^{19}F bond, the spectrum becomes a doublet (the components may have different intensities) governed by the *J* coupling, and a manifold of spinning sidebands determined by the interplay of dipolar, chemical shift anisotropic, and *J*-coupling interactions.[20]

Figure 1 shows ^{13}C spectra for sI (Fig. 1(a)), sII (Fig. 1(b)), and sH (Figs. 1(c) and 1(d)) hydrates containing CH_3F. The simplest spectrum is that for the sII hydrate, Figure 1(b), where the large H cages are occupied by THF

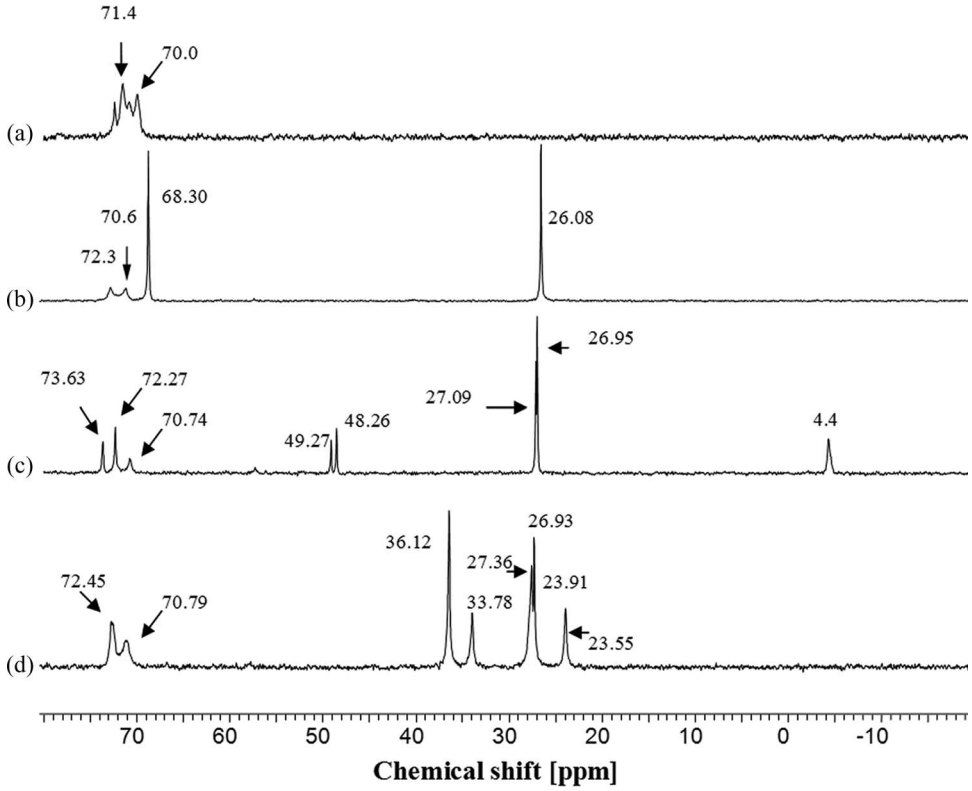

FIG. 1. ^{13}C HPDEC/MAS NMR spectra at 243 K of (a) sI CH_3F hydrate; (b) sII hydrate of CH_3F and THF; (c) sH hydrate of TBME with CH_3F and CH_4 in the small cages; and (d) sH hydrate with MCH and CH_3F as the small cage guest.

and CH_3F resides in the small D cages. The spectrum is a near-symmetric *J*-coupled doublet at 70–72 ppm with a splitting of 158 Hz. The small sII cage is nonspherical, however, the CH_3F rotational dynamics appear to be both fast and close to isotropic and shape complexities appear to be minimal. The peaks at ∼68 and ∼26 ppm correspond to THF in the large cage. The sI CH_3F spectrum, Figure 1(a), shows two overlapping doublets from molecules in large T and small D cages in the region between 70 and 73 ppm. The more intense doublet (70 and ∼71.4 ppm) can be attributed to CH_3F in the T large cage, which, similar to the ^{13}C spectrum of CH_4, has the small cage contribution to high field of that for the large cage. The large-cage doublet is asymmetric and this can be ascribed to interference effects. The spectrum for sH hydrate with both CH_3F and CH_4 in the small cages and TBME in the large cage is shown in Figure 1(c). Unfortunately, there is some excess liquid TBME in the sample at ∼28 ppm and at ∼49 ppm. The excess liquid TBME at ∼28 ppm overlaps with one of the CH_3F doublet components, the chemical shift at ∼48 ppm corresponds to TBME in the large cage.[19] The singlet CH_4 ^{13}C resonance at ∼−4 ppm is of interest. One might expect two lines, one for CH_4 in each D and D′ sH cavity, however, as will be shown below, there are some unexpected features in this system which can be ascribed to guest exchange dynamics which leads to a merging of the doublet peaks.[19] The spectrum of sH hydrate of MCH and CH_3F, Figure 1(d), shows a barely discernable asymmetric doublet for CH_3F, with a very small splitting at ∼26 ppm due to the slightly different chemical shifts of CH_3F in the D and D′ cage types. The spectrum between 20 and 40 ppm shows the chemical shifts of MCH in the large cage, there is some overlap with those of the liquid phase.[37] The ^{13}C NMR chemical shifts of CH_3F in the different clathrate hydrate structures are reported in Table I.

So far, with ^{13}C NMR spectra alone, it has not been possible to discern the cage preferences of CH_4 or CH_3F for the D and D′ cages of sH hydrate. As mentioned above, it was surprising to see a single line for CH_4 in the D and D′ cages of sH TBME hydrate with both CH_4 and CH_3F guests. A more detailed observation of the temperature dependence of the ^{13}C spectrum, concentrating on the small guest molecule regions is given in Figure 2. At the lowest temperature, 183 K, the CH_4 populations in the D and D′ cages are clearly distinguishable, although in the case of CH_3F a multiplet structure is observed. Measurement of the relative intensities shows that the ratio of the CH_4 populations $p(D')/p(D) = 0.53$. The usual value for this ratio is close to one if CH_4 is the only small cage guest, suggesting that there is a degree of partitioning with CH_3F having a small preference for the D′ cage. The CH_4 doublet collapses as the temperature is increased to ∼248 K. This was interpreted in terms of the CH_4

TABLE I. ^{13}C NMR chemical shifts (ppm with respect to TMS) at 243 K of the CH_3F guest incorporated into different clathrate hydrate structures.

Hydrate	System	^{13}C NMR shifts
sI	CH_3F	72.38, 71.46, 70.76, 70.00
sII	CH_3F-THF	72.33, 70.61
sH	CH_3F-MCH	72.27, 70.74
sH	CH_3F-CH_4-TBME	72.45, 70.79

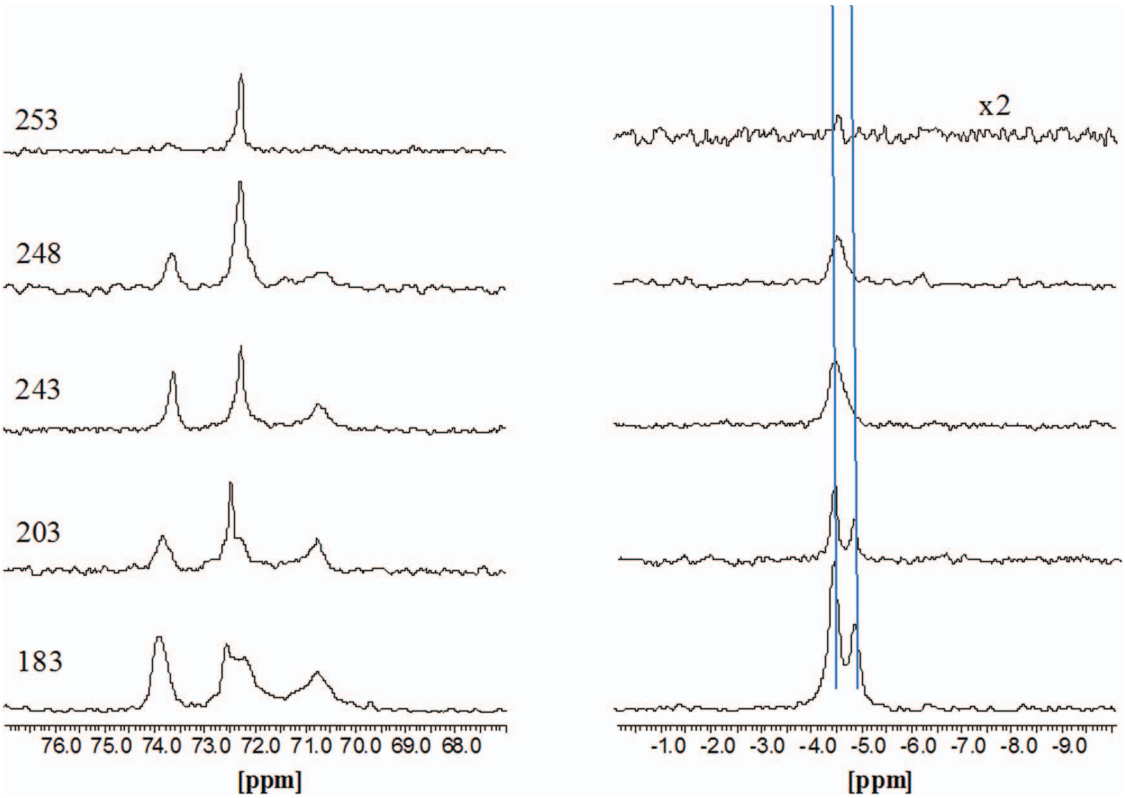

FIG. 2. Details of the ^{13}C NMR spectra of the sH TBME/CH_4/CH_3F hydrate as a function of temperature for the CH_3F (left hand side) and CH_4 (right hand side) guests. At 183 K, the separate spectral signatures of CH_3F and CH_4 in the D and D′ cages are clearly visible. However, by 243 K, the signals have coalesced, indicating that CH_3F and CH_4 in these cages are exchanging rapidly on a timescale determined by the chemical shift difference of the two signals in the slow motion limit.

populations in the D and D′ cages being able to exchange, thus averaging the chemical shift difference of 0.36 ppm (or 36 Hz at the Larmor frequency of the experiment). This process requires an exchange time greater than $\sim 4.4 \times 10^{-3}$ s, as the condition for a collapse of two signals separated in the absence of exchange by the chemical shift of 36 Hz is $1/2\pi \times 36$ ms. This direct observation of cage-to-cage guest exchange in the clathrate hydrate is relatively rare. While guest exchange between neighboring cages may occur in other systems, the timescales are too slow to be seen in the NMR spectrum. It was expected that the relatively rapid intercage dynamics may have some contributions from specific guest-host interactions, in particular related to the hydrogen bonding of TBME with the water lattice, as was the case for CO_2 dynamics in the binary THF sII clathrate hydrates.[4] Recent work,[30,38,39] after initial suggestions made many years ago,[40] has shown that guest molecules capable of accepting hydrogen bonds can introduce Bjerrum L-defects[41] in the water lattice by forming transient hydrogen bonds with a water molecule. Migration of L and D Bjerrum defects in the hydrate lattice occurs through water molecule reorientation.[40,41] Calculations have suggested that different small cage guests in sII hydrate can either enhance or retard the creation of Bjerrum defects.[4] Recent evidence based on high level *ab initio* calculations and structural and energetic analysis suggests that the F atom in CH_3F may act as a hydrogen bond acceptors in its complex with water.[42] The $CH_3F \cdots HOH$ binding energy was determined to be similar to water dimer and the $F \cdots H$ distance is 1.9926 Å which is consistent with hydrogen bonding. Special host-guest interactions[43] (i.e., halogen bonding[17] as, for example, in the hydrates of dihalogens),[44] may contribute to this hydrogen bonding so that the combination of TBME and CH_3F also may give rise to fast dynamics of the water lattice.

Recent calculations of CH_4 diffusivity in a hydrate lattice[44] have introduced water vacancies in the hydrate lattice in order to get reasonable rates of transport. Vacancies in the water lattice can be inferred as well from ^1H NMR studies of water molecular motion in THF[45] and ethylene oxide (EO)[46] hydrates, where the equivalent of centre-of-mass diffusion of water molecules was observed from the temperature dependence of the ^1H NMR line shapes and rotating frame relaxation time measurements. Whether such vacancies are intrinsic, or mediated by host-guest interactions remains unknown. The activation energy for water molecule diffusion in the two aforementioned hydrates is only ~20% less than it is in Ice Ih,[40] so it appears that the effect of guest-host interactions on water diffusion is rather smaller than it is on reorientation.

In order to further test the idea of cage-to-cage transport, a double hydrate of sII was prepared with THF and CD_3F as guests. CD_3F was employed to use the ^2H powder pattern to monitor the guest motions. The temperature dependence of the ^2H NMR powder pattern of CD_3F in the small cage of sII hydrate is shown in Figure 3. At 250 K, the doublet splitting gives a quadrupole coupling constant of 6.0 kHz, as compared with a value of 5.3 kHz for CD_3F in the large cage of sI

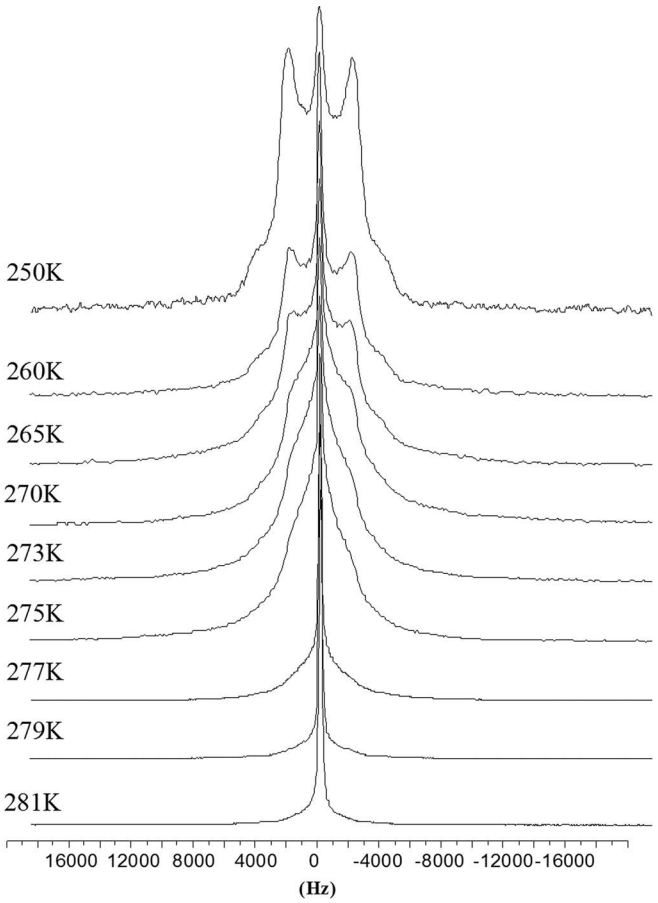

FIG. 3. ^{2}H NMR powder line shapes for CD_3F in the small cages of the sII double hydrate of THF and CD_3F. A quadrupolar coupling of 6 kHz is observed at 250 K. The line shape at 250 K was recorded last in order to confirm reversible behavior of the line shape. The disappearance of the doublet shows that the motion that sets in breaks the symmetry of the cage, hence is indicative of cage-to-cage transport.

hydrate at 268 K.[20] These rather similar values are characteristic of extensive motional averaging in the anisotropic sI large and the sII small cages. At 260 K, the powder pattern for the sII hydrate shows the start of further motional averaging which is reasonably complete at the highest temperature of study, 281 K. As observed before for CO_2 in the small cage of sII hydrate,[4] the motional averaging requires the breaking of the confining symmetry of the cage which can be achieved by the exchange of CH_3F among a number of different D cages, where some participating small cages in the diffusion process are empty. The minimum path for complete averaging of the quadrupolar tensor would be through a cluster of four neighboring D cages which are tetrahedrally arranged with respect to each other (a situation which exists in sII but not in sI or sH). The estimated correlation time for this motion is 3.5×10^{-5} s at 260 K.

Figure 4 shows ^{2}H NMR line shapes as a function of temperature for the sH hydrate of TBME and CD_3F. At 77 K the line shape is broad and featureless, characteristic of CD_3F guest dynamics in hydrate cages with frozen-in disorder of the water protons. At 160 K and higher temperatures the line shapes are considerably narrower with some discernible features. This means that even at 160 K, water dynamics is fast enough so that the hydrate cages have achieved their high average symmetry.[47] The D and D′ cages have quite different symmetries, one axial, the other non-axial (see Table II), so it should be possible to resolve the line shape contributions from guests in the two cages.

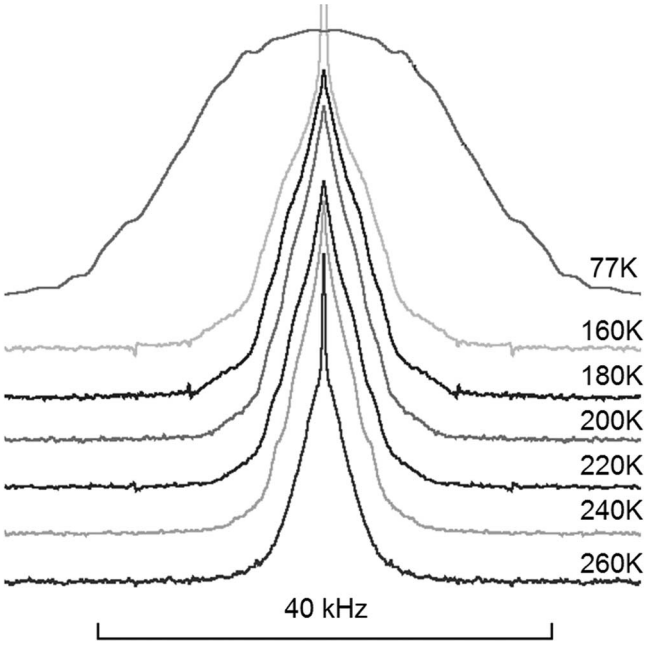

FIG. 4. ^{2}H NMR line shapes of CD_3F in the D and D′ cages of the sH hydrate of TBME/CD_3F as a function of temperature. The quadrupole coupling parameters are given in Table II.

Figure 5 shows the best visual fit when individual contributions from CD_3F in the D and D′ cage are added, varying the quadrupole coupling parameters as well as relative intensities. The symmetry of the D′ cage is such that the ^{2}H lineshape for CD_3F in this cage should have a zero asymmetry parameter. This was used as a constraint in the fitting.

Figure S1 of the supplementary material[36] shows an overlay of the ^{2}H NMR line shapes for the sH hydrates of TBME/CD_3F and TBME/CD_3F/CH_4. The difference spectrum lineshape has the same non-axial shape determined for CD_3F in the D cage in the fit shown in Fig. 5. This difference represents reduced intensity from CD_3F in the D cage in the CD_3F/CH_4/TBME hydrate, indicating that CD_3F has a slight preference for the D′ cage, whereas CH_4 shows a slight preference for the D cage.

The temperature dependence of the line shapes in Figure 4 gives some further insight into the dynamics at

TABLE II. ^{2}H NMR quadrupole coupling parameters of CD_3F in various cages.

Hydrate	Cage type	Cage symmetry	Quadrupole coupling constant Qc (kHz)	Asymmetry parameter (η)	T (K)
sI	D	m^3	0	0	261
sI	T	−42 m	5.3	0	261
sII	D	3 m	6.0	0	250
sH	D	mmm	5.1	0.7	200
sH	D′	−62 m	13.2	0	200

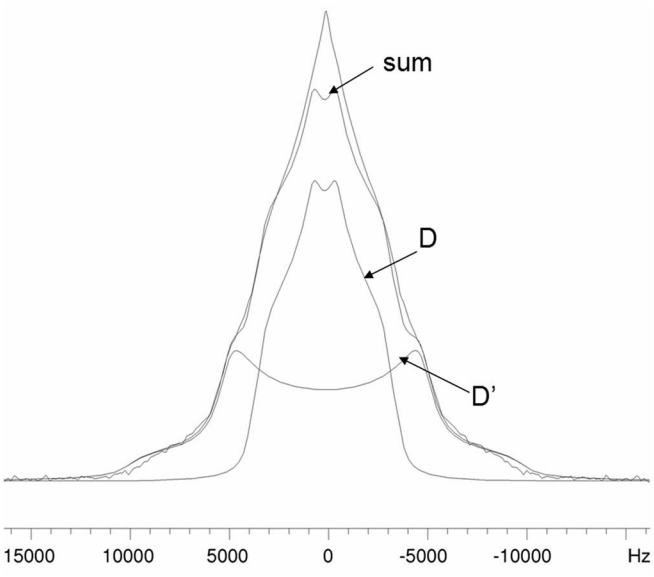

FIG. 5. Visual fit of the ^{2}H NMR spectrum at 200 K of the two contributions of CD_3F in the D and D′ cages of sH hydrate of TBME/ CD_3F. The quadruple coupling parameters of CD_3F in the various hydrates are shown in Table II.

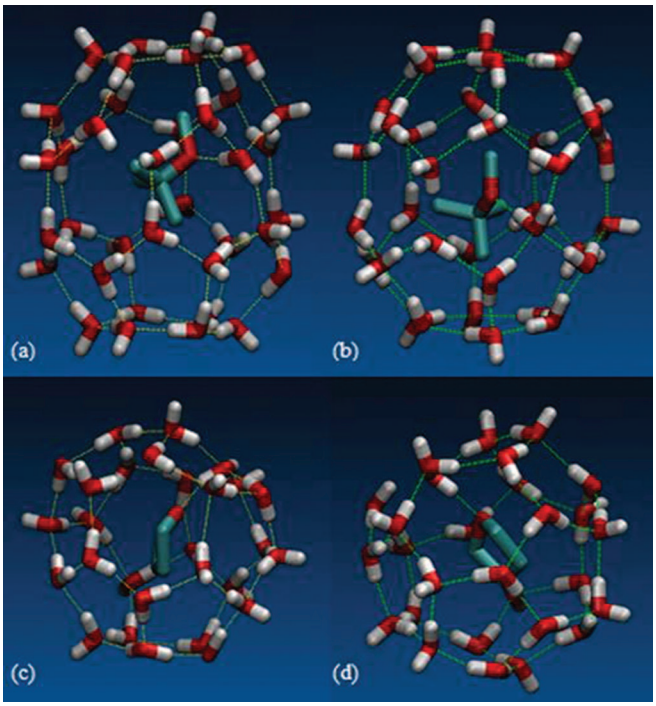

FIG. 6. Snapshots of the hydrogen bond formed between the TBME guest and the water molecule of the large cavity of sH (a) and (b) and the THF guest with the water molecule of the large cavity of sII (c) and (d). The sH snapshots are at 183 K and 1 bar, and the sII snapshots are at 250 K and 1 bar. (a) sH clathrate hydrate of CH_3F and TBME, (b) sH clathrate hydrate of CH_4 and TBME, (c) sII of CH_3 and THF, and (d) sII of CH_4 and THF. The hydrogen atoms of the guest molecules are not shown in these snapshots.

higher temperatures. Above ∼200 K the fine structure associated with the dynamics of the CD_3F molecules in the D and D′ cages starts to fade, and it is essentially gone at 260 K. Such disappearance of fine structure can be taken as a sign that the motion of the guest CD_3F molecules breaks the symmetry of the cage, as it would be expected if the CD_3F molecules in the D and D′ cages exchanged. In this case, if higher temperatures could be reached before decomposition one would expect to see a narrowed but structured lineshape. This is in agreement with the collapse of the ^{13}C NMR lines observed for CH_4 in the D and D′ cages in sH TBME/CH_3F/CH_4 hydrate at about 250 K in Figure 2.

B. MD studies

To understand some of the underlying microscopic behavior to the change in NMR spectra at different temperatures, we performed MD simulation studies of these systems with an emphasis on observing hydrogen bonding trends and guest dynamics. Hydrogen bonding was observed between framework water molecules and the ether atoms (OS) of the TBME and THF guests in the sH and sII large cages, respectively. Snapshots of hydrogen bonding configurations of these guests are shown in Figure 6. The radial distribution function (RDF) for the OS atoms of TBME and THF with the framework water hydrogen atoms (HW) and are shown in Figures S2 and S3, respectively, of the supplementary material.[36] The peaks in the OS-HW RDF at 1.8 Å in Figure S2 of the supplementary material[36] show the presence of guest-water hydrogen bonding in these systems. In the TBME hydrate, the height of the first peak in the OS-HW RDF is larger in the CH_3F binary hydrate than in the corresponding CH_4 binary hydrate which shows the greater probability of hydrogen bonding between TBME and water in the CH_3F binary hydrate. In all cases, guest-host hydrogen bonding increases at higher temperatures and there is only a small pressure dependence of the hydrogen bonding. In the case of the binary sII hydrates with THF, the first peaks in the OS-HW RDF which show the presence of guest-host hydrogen bonding, were smaller in both systems compared to the sH TBME OS-HW RDF peaks. However, even in the sII hydrate, the RDF peaks for the THF-water hydrogen bonding are higher in the binary hydrate with CH_3F than in the hydrate with CH_4.

The probability of hydrogen bonding between the large cage guests and water can be quantified by determining the fraction of snapshots in the simulation where the OS · · · HW distance is less than 2.1 Å. These probabilities are given in Table III. In the case of the TBME hydrates, the probabilities can also be determined from the integral

$$p = \int_0^{r_{\min}} \rho g(r) 4\pi r^2 dr, \qquad (2)$$

where $r_{\min}$ is the location of the first minimum after the peak which represents hydrogen bonding. These values are also given in Table III. In general, the hydrogen bonding probability in the CH_3F clathrate hydrates is greater than the corresponding CH_4 clathrate hydrates, it also increases at higher temperatures and decreases at higher pressures. The enhanced hydrogen bonding probability introduces a greater number of Bjerrum defects into the lattice.

In the present simulations, D and D′ cage vacancies were not introduced in the simulations and therefore direct migrations of CH_3F or CH_4 molecules between neighboring small cages (as inferred from the NMR results) are not observed.

TABLE III. Hydrogen bonding probabilities (p(H-bond)) of TBME and THF in binary sH and sII clathrate hydrates of CH_3F or CH_4 under different temperature and pressure conditions.

Clathrate	p(H-bond)	p_{RDF}(H-bond)	Clathrate	p(H-bond)	p_{RDF}(H-bond)
TBME+CH_3F			TBME+CH_4		
T = 183 K			T = 183 K		
p = 1 bar	0.7229	0.7581	p = 1 bar	0.2617	0.3057
p = 25 bar	0.6746	0.5708	p = 25 bar	0.3188	0.4326
p = 50 bar	0.5505	0.5708	p = 50 bar	0.1201	0.2325
T = 253 K			T = 253 K		
p = 1 bar	0.7286	0.8580	p = 1 bar	0.4299	0.7369
p = 25 bar	0.6358	0.9197	p = 25 bar	0.7158	0.7604
p = 50 bar	0.3363	0.9565	p = 50 bar	0.5612	0.7416
THF+CH_3F			THF+CH_4		
T = 250 K			T = 183 K		
p = 1 bar	0.0643	0.0722	p = 1 bar	0.0127	0.0057
T = 281 K			T = 183 K		
p = 1 bar	0.1499	0.1538	p = 1 bar	0.0290	0.0447

However, the contribution of hydrogen bonds of TBME with water on the migration of CH_3F and CH_4 between different cages can partly explain the difference observed between the ^{13}C spectra of the TBME + CH_3F/CH_4 hydrate of Figure 1(c) and the MCH + CH_3F hydrate of Figure 1(d). The MCH molecule does not have hydrogen bonding functional groups and CH_3F peaks in the sH small and medium cages in the ^{13}C spectrum retained their doublet structure. The CH_3F guest exchange between the D and D′ cages, if present in the MCH + CH_3F hydrate, occurs on a time scale slower than the NMR experiment.

Due to the non-polarizable force field used for CH_3F, we did not directly observe hydrogen bonding between fluoromethane and water. More accurate force fields can capture this additional contribution of fluoromethane to the dynamics of the clathrate hydrate phases.

The free energy of substitution of the CH_4 molecules for CH_3F in the binary sH clathrate hydrate, with TBME as the large cage guests, from thermodynamic integration at different temperature and pressure conditions are given in Table IV and Figure S4 of the supplementary material[36] shows the variation of $\langle \partial U(\lambda)/\partial\lambda \rangle_{T,p}$ as a function of the coupling parameter λ for Eq. (1). Details of the thermodynamic integration process are given in the supplementary material.[36] The configurational energy of the sH hydrate with TBME and CH_4 and TBME and CH_3F at various pressures and temperatures are also given in Table IV. Most of the results in Table IV indicate a small preference for CH_4 over CH_3F in the D and D′ sH clathrate hydrate cages, which could be due to the larger effective radius of CH_3F which makes its incorporation in the D and D′ cages more difficult. The thermodynamic preference for CH_4 may also be due to the destabilizing effect of the additional hydrogen bonding of the TBME guest with water when CH_3F is the small guest, see Table III.

To determine the effect of the guest size on the dynamics in the small and medium cages, we studied the velocity autocorrelation function (VACF) of CH_3F and CH_4 in the sH and sII clathrate hydrates. The VACF of the C atom is shown in Figures 7 and 8, while the VACF of the

TABLE IV. Configurational energy of sH hydrate with TBME and CH_4 and TBME and CH_3F and at various pressures and temperatures and free energy per unit cell of the chemical substitution of CH_4 with CH_3F under different pressure and temperature conditions. Assuming both species are ideal gases under the pressure and temperature conditions, this will be the total free energy for the substitution reaction.

Temperature (K)	Pressure (bar)	$E_{config}(CH_4)$ (kcal mol^{-1})	$E_{config}(CH_3F)$ (kcal mol^{-1})	ΔG_{TI} (kcal mol^{-1})
183	1	−459.07	−465.36	2.95
183	25	−462.81	−466.10	2.95
183	50	−460.07	−465.23	2.95
253	10	−435.02	−440.31	3.03
253	25	−435.96	−441.23	0.23
253	50	−436.96	−441.50	−1.97
263	25	−435.70	−436.84	2.24
274	24.5	−431.75	−433.43	0.09
280	25	−429.52	−427.60	2.38

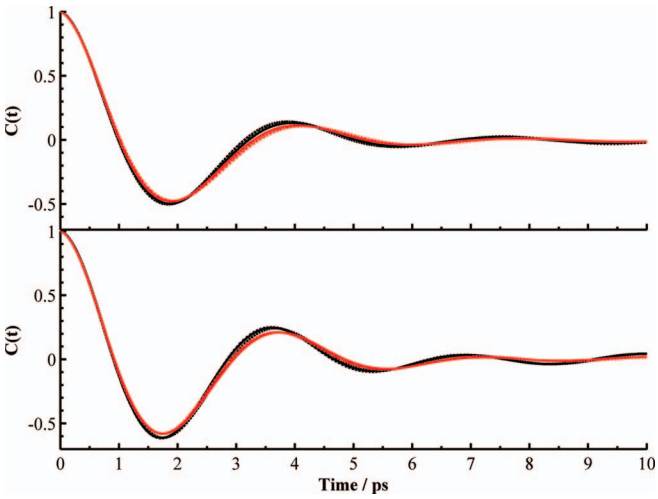

FIG. 7. The VACFs of the C atom of CH_3F (top) and CH_4 (bottom) in the D and D′ cages of sH clathrate hydrate with TBME as large cage guest at 183 K black curves and 253 K red curves.

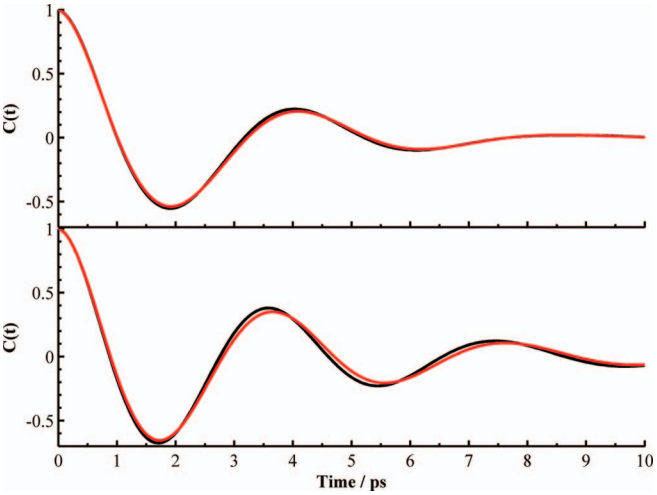

FIG. 8. The VACFs of the C atom of CH_3F (top) and CH_4 (bottom) in the D cages of sII clathrate hydrate with THF as large cage guest at 250 K black curves and 281 K red curves.

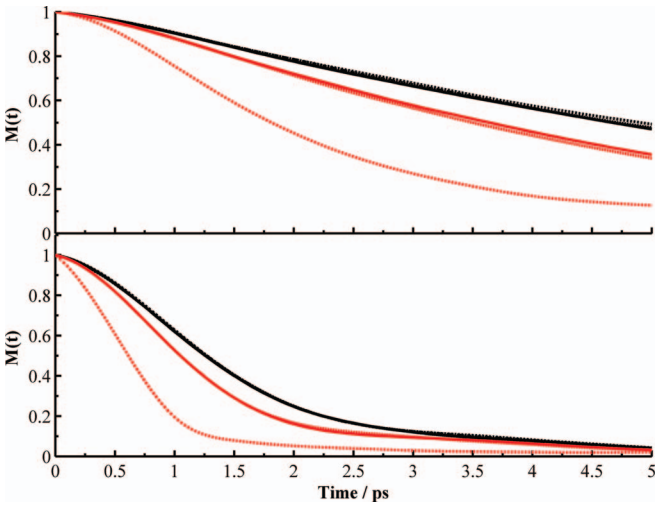

FIG. 9. The decay of the OACF $M(t)$ with time for CH_3F (top) and CH_4 (bottom) in the sH TBME hydrates at 183 K black curves and 253 K red curves. The full lines correspond to 1 bar, the dotted lines to 25 bar, and the dashed lines to 50 bar.

OS atom is shown in Figures S5–S6 of the supplementary material.[36]

The VACF for the carbon atoms of the CH_3F and CH_4 in the small and medium cages of the binary sH clathrate hydrate of TBME at different temperatures and pressures are shown in Figure 7. The long-time behavior of the VACF shows that the smaller CH_4 molecules have a higher frequency for rattling motion inside the cage.

The VACF for the carbon atoms of the CH_3F and CH_4 in the small cages of the binary sII clathrate hydrate of THF at different temperatures are show in Figure 8. Once again, the smaller CH_4 guests have a higher rattling frequency in the cages.

The VACF for the OS atom of TBME in the binary hydrates is shown in Figure S5 of the supplementary material.[36] The high hydrogen bonding probability of the TBME molecule with the cage water molecules in both binary hydrates (see Table III) indicates that this molecule will be tethered to the cage wall and undergo small high frequency vibrational motions in the large sH cages.

The VACF for the OS atom of THF in the binary hydrates is shown in Figure S6 of the supplementary material.[36] The hydrogen bonding probability of THF with the cage water molecules in the sII binary hydrates is smaller (see Table III) and the THF molecule mostly undergoes free rattling motion in the cage. The VACFs for the OS atoms of THF are much smoother than those of TBME. It is interesting to note that at 281 K, the VACF for THF in the binary hydrate with CH_3F undergoes a noticeable increase in rattling frequency, which correlates with a doubling of hydrogen bond probability at this temperature compared to the 250 K simulation.

The nature of the VACF for the different hydrates and the changes in guest dynamics at higher temperature correlate well with the changes in the NMR lineshapes and are among the complex changes that occur as the temperature of the hydrate is increased. As mentioned previously, the MD simulations span too short a time period to observe the direct D and D′ cage guest exchange between full and empty cages, but nonetheless, they do capture other features which may contribute to the occurrence and rate of guest exchange.

The orientation autocorrelation function (OACF), $M(t)$ of the CH_3F and CH_4 molecule in the small cage is a measure of the rotation of a unit vector $\mathbf{u}(t)$ in the direction of the C–F bond for CH_3F or C–H for CH_4 at each time t with respect to a time origin, $\mathbf{u}(0)$,

$$M(t) = P_1 [\cos\theta(t)] = \langle \mathbf{u}(t) \cdot \mathbf{u}(0) \rangle . \quad (3)$$

The $M(t)$ represents the ensemble average of P_1 which is the first order Legendre polynomial. At any time, $\mathbf{u}(t) \cdot \mathbf{u}(\mathbf{0}) = \cos\theta(t)$ represents the angle a molecule has rotated by time t and the brackets represent the ensemble average. It can be observed in Figures 9 and 10 that the decay of $M(t)$ for CH_4 is

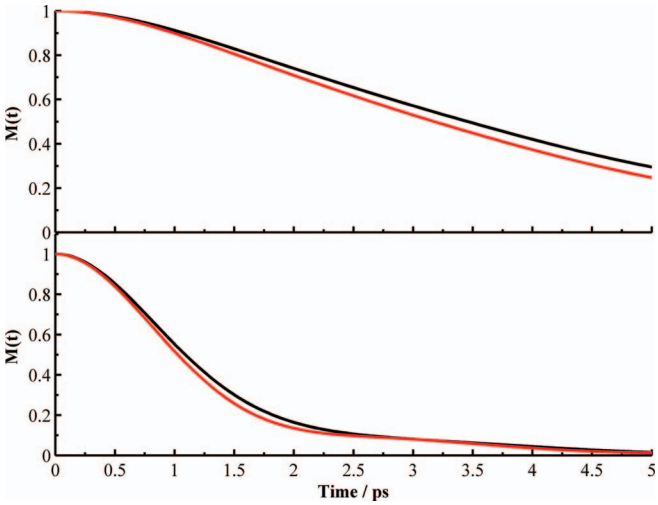

FIG. 10. The decay of the OACF $M(t)$ with time for CH_3F (top) in the sH TBME and sII THF hydrates and CH_4 (bottom) in the sH TBME and sII THF hydrates at 250 K black curves and 281 K red curves.

faster than that of CH_3F in both hydrate structures. The orientation vector $\mathbf{u}(t)$ of CH_3F maintains its original direction for longer times, whereas CH_4 rotates more freely. As expected, both decays are more rapid at higher temperatures. The larger size of the CH_3F molecule hampers its rotational motion compared to the smaller CH_4 molecule.

IV. CONCLUSIONS

The ^{13}C NMR studies show the incorporation of fluoromethane and methane as help-gas species in the D and D′ cages of sH and D cages of sII binary clathrate hydrates with TBME and THF, respectively. At low temperatures, the ^{13}C NMR peaks associated with CH_3F show doublet structures, reflecting the non-spherical environments of the sII and sH cages. At high temperature, beginning at ∼250 K, these doublet peaks merge into a single peak which implies a local migration of CH_3F and CH_4 between neighboring cages. The sH clathrate hydrate of CH_3F with the methylcyclohexane does not show the merging of the doublet of peaks. Molecular dynamics simulations show that the TBME and THF guest molecules have enhanced hydrogen bonding in the binary hydrates with CH_3F which could be due to the larger size of these molecules and the resulting weakening of the water hydrogen bonding network in the cages which accommodate CH_3F, which then enhances the hydrogen bonding with the large cage guests.

The ^2H NMR powder lineshapes of the THF/CD_3F hydrate at different temperatures also show the transformation of the low temperature doublet peak of CD_3F into a single isotropic peak at temperatures above 270 K or so. This verifies the picture of cage-to-cage transport of the small guests.

Molecular dynamics simulations show the role of the small/medium cage guests on the hydrogen bonding of the large cage guests with the hydrate framework water molecules. The larger CH_3F molecule, which also has a non-zero dipole moment, interacts with the cage water molecules to a greater extent, leading to slower translational and rotational dynamics of this molecule in the D and D′cages. This in turn leads to greater hydrogen bonding probability of the large guests in the binary hydrates which have CH_3F as the help-gas. Hydrogen bonding between fluoromethane that have been observed in high level quantum chemical calculations may also contribute to the experimentally observed dynamics of the fluoromethane containing clathrate hydrate phases.

^2H NMR lineshapes and molecular dynamics thermodynamic integration free energy calculations show that there is a small systematic preference for CH_4 in the D and D′ cages compared to CH_3F.

ACKNOWLEDGMENTS

The authors gratefully acknowledge the financial support of the ACTS Sustainable Hydrogen Program, Reg. No. H2 2007. We thank S. Lang for technical support.

[1]D. W. Davison, *Water: A Comprehensive Treatise* (Plenum Press, New York, 1973), Vol. 2.
[2]G. A. Jeffrey, *Comprehensive Supramolecular Chemistry* (Pergamon/Elsevier, London, 1996), Vol. 6.
[3]G. A. Jeffrey, *Inclusion Compounds* (Academic Press, London, 1984), Vol. 1.
[4]S. Alavi and J. A. Ripmeester, J. Chem. Phys. **137**, 054712 (2012).
[5]D. W. Davidson, S. K. Garg, S. R. Gough, Y. P. Handa, C. I. Ratcliffe, J. A. Ripmeester, J. S. Tse, and W. F. Lawson, Geochim. Cosmochim. Acta **50**, 619 (1986).
[6]H. L. Lu, Y. T. Seo, J. W. Lee, I. Moudrakovski, J. A. Ripmeester, N. R. Chapman, R. B. Coffin, G. Gardner, and J. Pohlman, Nature (London) **445**, 303 (2007).
[7]Y. Seo, H. Tajima, A. Yamasaki, S. Takeya, T. Ebinuma, and F. Kiyono, Environ. Sci. Technol. **38**, 4635 (2004).
[8]K. Shiojiri, T. Okano, Y. Yanagisawa, M. Fujii, A. Yamasaki, H. Tajima, and F. Kiyono, in *Carbon Dioxide Utilization for Global Sustainability*, edited by S. E. Park, J. S. Chang, and K. W. Lee (Proceedings of the 7th International Conference on Carbon Dioxide Utilization, Korea, 2004), p. 507.
[9]P. Englezos and J. D. Lee, Kor. J. Chem. Eng. **22**, 671 (2005).
[10]M. Nohra, T. K. Woo, S. Alavi, and J. A. Ripmeester, J. Chem. Thermodyn. **44**, 5 (2012).
[11]J. S. Gudmundsson, M. Parlaktuna, and A. A. Khokhar, SPE Prod. Facil. **9**, 69 (1994).
[12]S. Alavi, K. Udachin, C. I. Ratcliffe, and J. A. Ripmeester, *Supramolecular Chemistry* (John Wiley & Sons, Ltd., 2012).
[13]I. L. Moudrakovski, G. E. McLaurin, C. I. Ratcliffe, and J. A. Ripmeester, J. Phys. Chem. B **108**, 17591 (2004).
[14]M. J. Collins, C. I. Ratcliffe, and J. A. Ripmeester, J. Phys. Chem. **94**, 157 (1990).
[15]D. W. Davidson, C. I. Ratcliffe, and J. A. Ripmeester, J. Inclu. Pheno. **2**, 239 (1984).
[16]T. Uchida, R. Ohmura, and A. Hori, J. Phys. Chem. C **112**, 4719 (2008).
[17]S. Takeya, and R. Ohmura, J. Chem. Eng. Data **52**, 635 (2007).
[18]S. Takeya, K. Yasuda, and R. Ohmura, J. Chem. Eng. Data **53**, 531 (2008).
[19]R. Susilo, J. A. Ripmeester, and P. Englezos, Chem. Eng. Sci. **62**, 3930 (2007).
[20]K. W. Zilm and D. M. Grant, J. Am. Chem. Soc. **103**, 2913 (1981).
[21]S. A. Carss, R. K. Harris, and R. A. Fletton, Magnet. Reson. Chem. **33**, 501 (1995).
[22]S. Alavi, J. A. Ripmeester, and D. D. Klug, J. Chem. Phys. **123**, 024507 (2005).
[23]S. Alavi, J. A. Ripmeester, and D. D. Klug, J. Chem. Phys. **125**, 104501 (2006).
[24]S. Alavi, J. A. Ripmeester, and D. D. Klug, J. Chem. Phys. **126**, 124708 (2007).
[25]P. Dornan, S. Alavi, and T. K. Woo, J. Chem. Phys. **127**, 124510 (2007).
[26]J. H. Davis, K. R. Jeffrey, M. Bloom, M. I. Valic, and T. P. Higgs, Chem. Phys. Lett. **42**, 390 (1976).
[27]W. Smith, T. R. Forester, I. T. Todorov, *The DL_Poly_2 User Manual, Version 2.20*, 2010.
[28]S. Nose, J. Chem. Phys. **81**, 511 (1984).
[29]S. Sasaki, S. Hori, T. Kume, and H. Shimizu, J. Chem. Phys. **118**, 7892 (2003).
[30]S. Alavi, R. Susilo, and J. A. Ripmeester, J. Chem. Phys. **130**, 174501 (2009).
[31]J. D. Bernal and R. H. Fowler, J. Chem. Phys. **1**, 515 (1933).
[32]J. L. F. Abascal, E. Sanz, R. G. Fernandez, and C. Vega, J. Chem. Phys. **122**, 234511 (2005).
[33]M. J. Frisch, G. W. Trucks, H. B. Schlegel *et al.*, GAUSSIAN 03, Revision B.04, Gaussian, Inc., Pittsburgh, PA, 2003.
[34]D. A. McQuarrie, *Statistical Mechanics* (Harper & Row, New York, 1976).
[35]K. E. G. S. Murad, *Computer Modeling of Matter*, ACS Symposium Series Vol. 86 (American Chemical Society, 1978) .
[36]See supplementary material at http://dx.doi.org/10.1063/1.4874636 for short description of free energy calculations, Figs. S1–S6 and Table S1.
[37]J. W. Lee, H. L. Lu, I. L. Moudrakovski, C. I. Ratcliffe, R. Ohmura, S. Alavi, and J. A. Ripmeester, J. Phys. Chem. A **115**, 1650 (2011).
[38]S. Alavi, K. Udachin, and J. A. Ripmeester, Chem.-Eur. J. **16**, 1017 (2010).
[39]R. Susilo, S. Alavi, I. L. Moudrakovski, P. Englezos, and J. A. Ripmeester, ChemPhysChem **10**, 824 (2009).

[40]D. W. Davidson and J. A. Ripmeester, *Inclusion Compounds: Physical Properties and Applications* (Academic Press, 1984), Vol. 3.
[41]N. Bjerrum, Science **115**, 385 (1952).
[42]R. E. Rosenberg, J. Phys. Chem. A **116**, 10842 (2012).
[43]K. A. Udachin and J. A. Ripmeester, "Unpublished results on structure of CH_3F hydrate," Steacie Institute for Molecular Sciences, National Research Council, Canada, (2013).
[44]B. Peters, N. E. R. Zimmermann, G. T. Beckham, J. W. Tester, and B. L. Trout, J. Am. Chem. Soc. **130**, 17342 (2008).
[45]S. K. Garg, D. W. Davidson, and J. Ripmeester, J. Mag. Reson. **15**, 295 (1974).
[46]J. A. Ripmeester, Can. J. Chem.-Rev. Can. Chim. **54**, 3677 (1976).
[47]J. A. Ripmeester and C. I. Ratcliffe, J. Struct. Chem. **40**, 654 (1999).